Soft Wearable Pressure Sensors for Beat-to-Beat Blood Pressure Monitoring

Joshua Kim, En-Fan Chou, Jamie Le, Sabrina Wong, Michael Chu, and Michelle Khine*

Wrinkled gold thin films on elastomeric substrates are used as robust parallel plate electrodes for soft capacitive pressure sensors. The wrinkled structures create a robust integration with the polymer, allowing repeated normal force to deform the thin film without failure. By incorporating microridged structures that support the counter electrodes to create air cavities within the elastomeric dielectric layer, pressure sensitivity is further increased to 0.148 kPa^{-1} over a wide dynamic range of up to 10 kPa. The wide dynamic range and pressure sensitivity of the pressure sensor allow for consistent measurements of the pressure exerted by the radial artery located on the wrist. The soft capacitive pressure sensor displays comparable results when tested against an FDA approved device (Clearsight, Edwards Lifesciences, Irvine, CA) measuring beat-to-beat blood pressure. These soft pressure sensors using wrinkled thin films, therefore, illustrate considerable potential to continuously monitor beat-to-beat blood pressure.

1. Introduction

The arterial pulse contains a wealth of cardiovascular information, including systolic and diastolic pressures, that have clinically been used to quantitatively evaluate and monitor cardiovascular diseases as well as general health.[1] These arterial pulses can be measured in many different locations of the body, such as the brachial and radial artery, using noninvasive blood pressure (NIBP) monitoring tools. Studies have indicated that monitoring blood pressure fluctuations throughout the day can provide insight on cardiovascular health.[2–7] For this reason, there is a need to continuously monitor blood pressure to better understand blood pressure variability and its effect on cardiovascular health.

Oscillometric measurements, using inflatable brachial arm cuffs, have become widely used in the clinical setting, but are intermittent and only provide one systolic and diastolic blood pressure value over a duration of ≈30–40 s.[8–10] Alternatively, continuously monitoring beat-to-beat blood pressure requires detection and analysis of each cardiac cycle as it pulses to peripheral arteries. The finger cuff volume-clamp method[9–11] is one such method capable of measuring beat-to-beat blood pressure, but currently does not have the form factor to enable ambulatory monitoring. Arterial applanation tonometry is another NIBP method that uses a pressure sensor, often a hand-held probe, to locally flatten (applanate) an artery.[10,12,13] Subsequently, the arterial pressure is measured by adjusting the degree of arterial applanation. Applanation tonometry greatly depends on the operator to consistently position the pressure transducer on the artery to measure pulse pressure which is not amenable for ambulatory continuous monitoring. Newer alternative methods use soft sensors that are capable of improving conformability to the body.[14–17] Conformability improves the coupling between the sensor and body allowing for more accurate measurements of the arterial pulse.[18] However, current reported soft sensors measure pulse transit times between two points as a means to calculate beat-to-beat blood pressure using theoretical models and not from the amplitude changes of the pulse pressure waveforms.

Researchers have developed flexible wearable capacitive pressure sensors with improved device form factors that are potentially more compatible for ambulatory monitoring in contrast with current radial applanation tonometry technologies.[18–23] Capacitive pressure sensors have gained much attention due to their simple device design, quick response times, relatively low hysteresis, and low power consumption requirements, which are all highly desirable for soft wearable electronic applications. When soft dielectric materials are used, compression of the dielectric layer will lead to an increased capacitance, which is equal to

$$C = \varepsilon_o \varepsilon_r \frac{A}{d} \tag{1}$$

where ε_o is the permittivity of vacuum, ε_r is the relative permittivity of the dielectric material, A is the surface area overlap of the parallel plate electrodes, and d is the distance between the parallel plate electrodes.

Capacitive pressure sensors are typically characterized with low pressure sensitivities due to the small compression of the

Dr. J. Kim, Prof. M. Khine
Department of Materials Science and Engineering
University of California Irvine
Irvine, CA 92697, USA
E-mail: mkhine@uci.edu
E.-F. Chou, J. Le, S. Wong, M. Chu, Prof. M. Khine
Department of Biomedical Engineering
University of California Irvine
Irvine, CA 92697, USA

The ORCID identification number(s) for the author(s) of this article can be found under https://doi.org/10.1002/adhm.201900109.

ADVANCED
SCIENCE NEWS
www.advancedsciencenews.com

ADVANCED
HEALTHCARE
MATERIALS
www.advhealthmat.de

dielectric layer, which impacts arterial pulse measurements. For example, Lipomi et al. developed skin-like capacitive pressure sensors using elastic carbon nanotube (CNT) conductors supported on polydimethylsiloxane (PDMS) substrates.[24] Although these conductors were supported on soft substrates with skin-like properties, the reported capacitive pressure sensor had low pressure sensitivities, which would have made it difficult to measure arterial pulse pressures.

Mannsfeld et al. have reported capacitive pressure sensors incorporating PDMS micropyramidal structures in the dielectric layer to significantly improve pressure sensitivities.[25] Pang et al. also incorporated microhairy PDMS structures to improve conformability to the surface of the skin, subsequently amplifying arterial pulse pressure measurements.[18] They have demonstrated that by applying more pressure down on the sensor into the skin they were able to achieve slightly larger changes in the radial arterial pulse pressure waveform. However, these changes were minimal, possibly suggesting that the dynamic range of the pressure sensors were not sufficient for applanation tonometry.

Arterial applanation is a critical component to achieving consistent pulse pressure measurements by reducing the elastic resistance (i.e., skin) between the pressure sensor and the artery.[26,27] To achieve arterial applanation and consistent pulse pressure measurements requires the pressure sensor to have high pressure sensitivities over a wide dynamic range. One such way to achieve a wide dynamic range in soft capacitive pressure sensors includes creating air gaps with microridged structures.

Here, we introduce soft capacitive pressure sensors that incorporate highly wrinkled Au (wAu) thin films to develop soft stretchable electrodes for radial tonometry applications as shown in **Figure 1**. The parallel plates can be seen visibly coming closer together when the radial artery induces pressure on the sensor (Movie S1, Supporting Information). The wrinkled structures of the Au thin film create robustness for the thin film to repeatedly flex (Figure 1b). This enables continuous arterial pulse pressure measurements with enough sensitivity over a large dynamic range (**Figure 2**) and fast response times

of less than 10 ms (Figures S1 and S2, Supporting Information) to capture the details of the pulse pressure waveform (**Figure 3**).

As previously reported, highly wrinkled thin films provide mechanical robustness to mechanical strains when supported on soft elastomeric substrates.[28–30] Due to the soft nature of these electrodes, it is possible for the sensors to conform to the body and accurately measure pressure from an arterial pulse. To increase pressure sensitivity and dynamic range, we also include microridged structures in the dielectric layer to improve pressure sensitivities of up to fivefold within a wide pressure range from 0 to 10 kPa. These microstructures lift up the counter electrode to create an air cavity in the dielectric layer, thereby increasing the amount the dielectric layer can be compressed (Figure 1c). In effect, this reduces the elastic resistance in the dielectric layer. The effective dielectric permittivity is also lowered due to the presence of an air cavity ($\varepsilon_{air} = 1$). When the dielectric layer is compressed, the effective dielectric permittivity increases as the air cavity volume decreases leading to larger changes in capacitance.[18,25] We demonstrate continuous measurements of beat-to-beat blood pressure with these soft capacitive pressure sensors by comparing against an FDA approved NIBP monitoring device (**Figure 4**).

2. Results and Discussion

2.1. Sensor Fabrication

Soft capacitive pressure sensors comprised of two conductive parallel plates separated by a dielectric layer were fabricated using a previously reported thermally induced shrinking fabrication process (Figure S3, Supporting Information).[28–30] We have previously shown that it is possible to form highly wrinkled structures in Au (wAu) thin films when shrunk on polystyrene (PS) substrates. When these wrinkled thin film structures were transferred onto silicone elastomeric substrates, the wAu thin film demonstrated stretchability of up to 200% before electrical failure.[28]
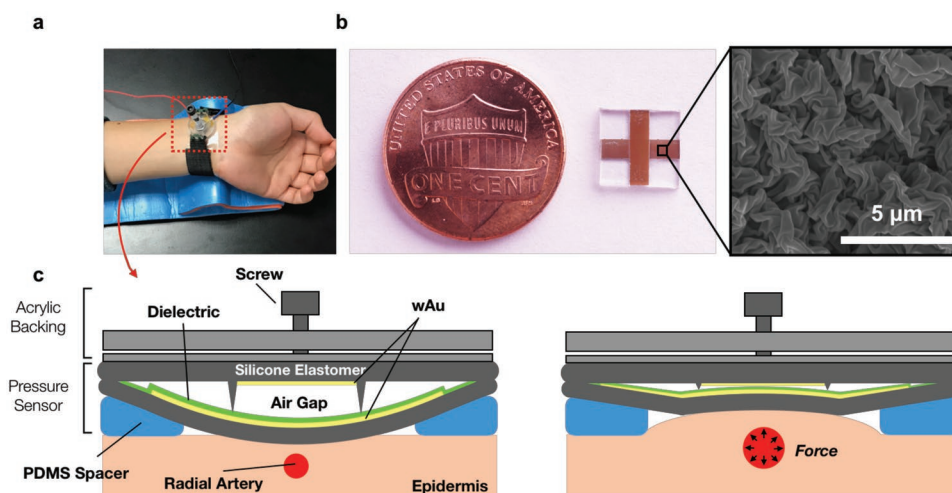

Figure 1. a) Image of how the pressure sensor is attached to the wrist. Photograph image of the parallel wAu electrodes. b) Photographic image of capacitive pressure sensor and a scanning electron microscope (SEM) image of the wAu. c) Schematic illustration of the pressure sensor when placed on the wrist above the radial artery. On the right, pressure sensor is deformed as blood pulses through the radial artery. Screw is used to add incremental pressure to applanate the radial artery.
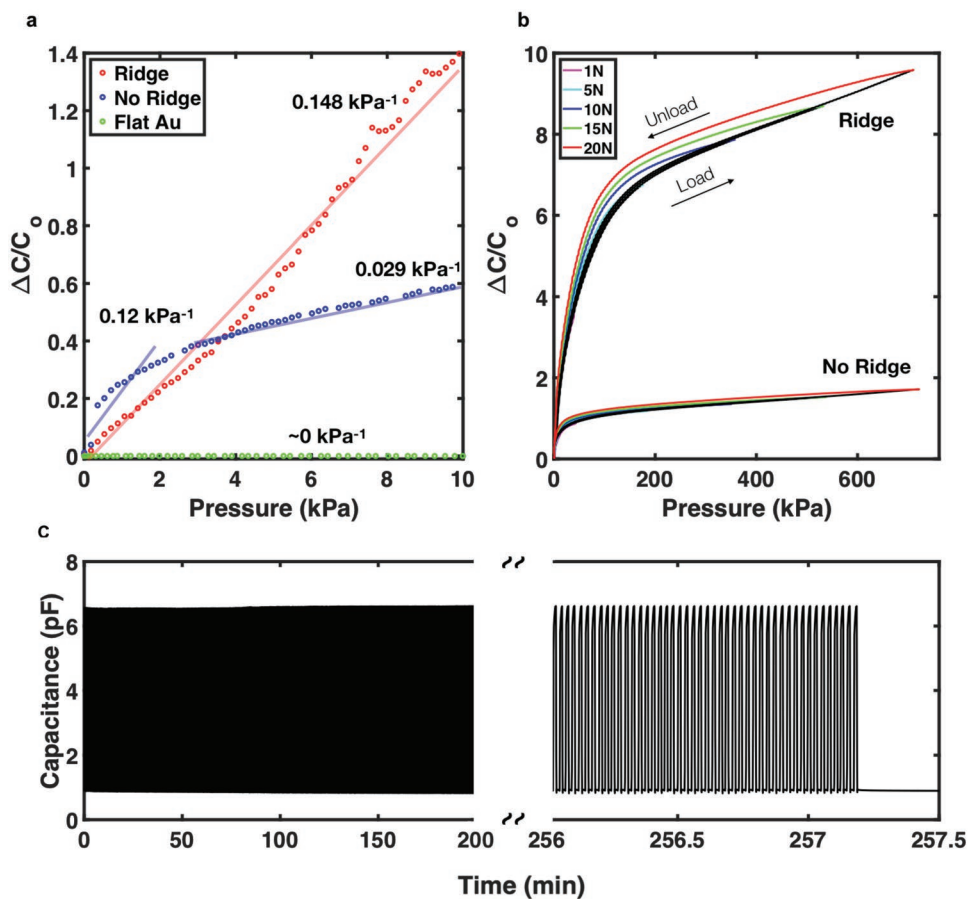
Figure 2. a) Pressure sensitivity curve from 0 to 10 kPa of capacitive pressure sensor with ridge (red), no ridge (blue), and sensor made with flat Au electrodes (green). b) Pressure sensitivity curve of the pressure sensor with the ridge versus with no ridge. Black lines indicate the loading, and the colored lines indicate the unloading. The amount of load that was applied prior to unloading is indicated by the colored lines in Newtons. c) Cyclic load of 25 kPa over 5000 cycles.
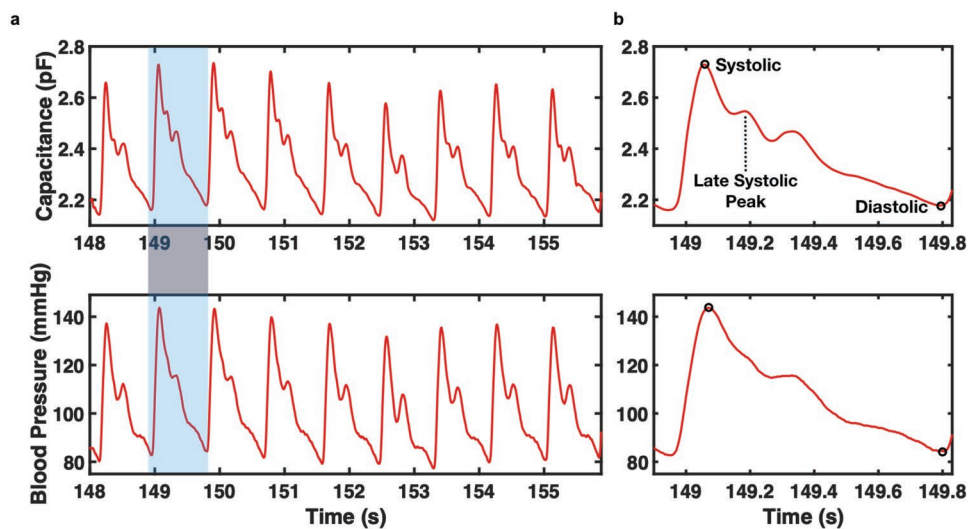

Figure 3. a) Example of arterial pulse waveforms measured by the capacitive pressure sensor (top row) and the Clearsight device (bottom row). b) Inset of one pulse waveform indicating cardiovascular features.
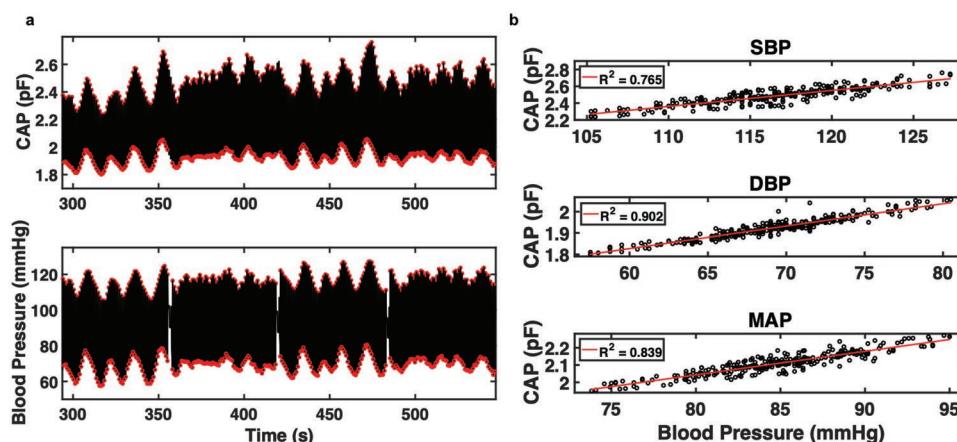
Figure 4. a) Example of the four 70 beat sections from Subject 1 that were used to compare between the capacitive pressure sensor and the Clearsight. Arterial pulse waveforms are shown in black and highlighted in red indicate the SBP and DBP. b) Linear regression analysis of SBP, DBP, and MAP between the pressure sensor and the Clearsight.

Due to mechanical robustness, these wAu electrodes were used as parallel plates (2 × 2 mm²) in the capacitive pressure sensor. These wrinkled structures significantly improve mechanical robustness allowing wAu thin films of 15 nm thickness to be integrated into soft substrates and withstand thousands of cycles. Notably, these electrodes are capable of being supported on soft silicone substrates, including PDMS, which are important to measure localized pressures.[31,32] Many reported capacitive pressure sensors use stiff substrates, such as polyethylene terephthalate (PET, $E \approx 2.5$ GPa), which are not as mechanically compatible to the human body as soft silicone elastomers, such as PDMS ($E \approx 1$ MPa[33,34]). Stiff substrates may also potentially hinder spatial resolution of localized stress and negatively impact arterial pulse measurements.

A soft silicone elastomer, Ecoflex (15 µm), was used as the soft dielectric layer between the parallel plates. Ecoflex was used due to its soft mechanical properties (shore hardness 00-30), as opposed to PDMS (shore hardness A-48), to reduce the elastic resistance between the parallel plate electrodes to improve pressure sensitivity.[24,35] In addition, microstructured ridges were made by molding laser cut etched grooves in the PS substrate with PDMS. Laser cutting is a rapid prototyping method that can be used to form microstructures quickly by etching and subsequently molding the etched grooves. The detailed fabrication process flow can be found in Figure S3 in the Supporting Information and also further explained in the Experimental Section. The microstructured ridges were ≈85 µm in height, 100 µm in width, and were spaced ≈2 mm between each other located adjacent to the edge of the wrinkled thin film electrode, which can be seen in Figure S4a in the Supporting Information. The air gap size between the electrodes was ≈130 µm in height seen in Figure S4b in the Supporting Information. The ridge supported the counter electrode creating an air cavity within the dielectric layer.

When pressure was applied, the parallel plates were brought closer together leading to an increased capacitance. Due to the compression of the air cavity, the effective relative permittivity

also increased closer to that of ε_{eco}, leading to larger changes in capacitance. This effect can be illustrated by Equation (2)[36]

$$\frac{\Delta C}{C_o} = \frac{\varepsilon_o \varepsilon_r (A/d)}{\varepsilon_o \varepsilon_{ro}(A/d_o)} - 1 = \frac{\varepsilon_r d_o}{\varepsilon_{ro} d} - 1 \qquad (2)$$

where ε_{ro} is the relative permittivity before added pressure, and ε_r is the relative permittivity after added pressure.

2.2. Electromechanical Characterization

The soft capacitive pressure sensor's electromechanical performance was evaluated by measuring pressure sensitivity, which is defined by Equation (3)

$$S = \frac{\Delta C/C_o}{P} \qquad (3)$$

where ΔC is the change in capacitance, C_o is the initial capacitance, and P is pressure. The pressure sensitivity of the sensor was measured by applying force and measuring the change in capacitance. The force was applied over a 6 mm fiber glass probe tip attached to a force gauge. The fiber glass probe was used to reduce any fringe capacitance interference with the capacitive pressure sensor.

The pressure sensitivity of pressure sensors with microstructured ridges measured was 0.148 kPa⁻¹ between 0 and 10 kPa (Figure 2a). A control of wrinkled electrodes with no microstructured ridges was also tested. The capacitive pressure sensor with no microridges was characterized with a lower pressure sensitivity of 0.029 kPa⁻¹ between 3 and 10 kPa. However, the pressure sensitivity of the pressure sensors with no ridges displayed a pressure sensitivity of around 0.12 kPa⁻¹ in the 0–2 kPa range, which is comparable to the pressure sensor with the microridges. In this case, although there are no microridges to create an air cavity, small air gaps are still present due to the roughness of the wrinkled Au electrodes. However, these air gaps are completely compressed in

ADVANCED
SCIENCE NEWS
www.advancedsciencenews.com

ADVANCED
HEALTHCARE
MATERIALS
www.advhealthmat.de

the low-pressure regions resulting in lower pressure sensitivities when additional pressure is applied. Therefore the microstructured ridges allow soft capacitive pressure sensors to achieve high pressure sensitivities over a wide dynamic range. However, when the microridge size increases (190 µm height; 600 µm width), the pressure sensitivity decreased (Figure S5, Supporting Information). This decrease in pressure sensitivity can be attributed to the larger features that need to be compressed.

Capacitive pressure sensor with flat Au electrodes was fabricated to compare against wAu electrodes. Due to the brittleness of Au thin films on PDMS substrates, 90 nm of Au was used instead of 15 nm as it was not possible to transfer the 15 nm. The capacitive pressure sensors with flat Au electrodes displayed pressure sensitivities of ≈0 kPa^{-1} from 0 to 10 kPa (which had little to no air gap present). This suggests that the wAu electrodes provide mechanical robustness allowing for depositions of thin films of as low as 15 nm, and also display significantly higher pressure sensitivities compared to flat Au electrodes.

Larger pressure ranges were also investigated and compared between sensors with and without the microstructured ridges. A mechanical load was first applied and then unloaded with 1 N (Figure S5, Supporting Information) displaying signs of hysteresis. This was then repeated with increasing loads from 1 to 20 N, as seen in Figure 2b. The electromechanical response of both conditions display characteristics of the Mullins effect, which states that the stress–strain curve depends on the magnitude of stress previously applied.[37] As seen in Figure 2b, the electromechanical response of the pressure sensor with microridges displayed higher pressure sensitivities over a wider dynamic range in comparison to the pressure sensor with no microridges.

In addition, the electromechanical response to cyclical loading was analyzed, as shown in Figure 2c. The pressure sensor was loaded with ≈25 kPa for 5000 cycles. As shown in Figure 2c, the pressure sensor shows mechanical robustness to stress over a large number of cyclic loads. This demonstrates durability to cyclic mechanical loading, which is necessary for continuous arterial pressure measurements.

It is evident that incorporation of microridges improved pressure sensitivities of up to fivefold within a wide dynamic range between 0 and 10 kPa. Even, without the microridges, the pressure sensitivities were significantly higher in comparison to pressure sensors without the wrinkled structures. In addition, the mechanical robustness of the wrinkled structures allowed for deposition of significantly thinner electrodes making it more facile and rapid to fabricate. Reproducibility of these sensors is shown in Figure S6 in the Supporting Information.

In addition, response and relaxation times of the pressure sensor were measured. A probe with ≈2 mm diameter was attached to a linear actuator which can be controlled by an Arduino. The pressure sensor displayed response times (<10 ms) and relaxation times (<17 ms) when applied with an impulse of strain (<1 ms) (Figure S1, Supporting Information). The pressure sensor was also capable of measuring cyclic strains of up to 10 Hz (Figure S2, Supporting Information). Sampling measurement rate used for dynamic mechanical tests was ≈130 Hz (4291B, Agilent, CA).

2.3. Beat-to-Beat Blood Pressure Monitoring

2.3.1. Experimental Setup for NIBP

As previously mentioned, arterial tonometry is a method to quantify arterial pulse pressure using pressure sensors. It is possible to monitor arterial pulse pressure using soft capacitive pressure sensors as well. Accurate and precise measurement of the radial arterial pulse pressure can then be translated into beat-to-beat blood pressure for NIBP wearable applications.

To demonstrate beat-to-beat blood pressure monitoring, we applied the sensors to healthy subjects under approval from the Institutional Review Board of the University of California (IRB no.2016-2924). One soft capacitive pressure was tested on a total of seven subjects to demonstrate robustness. Two additional soft capacitive sensors were tested on Subject 1 to demonstrate reproducibility. The pressure sensor was attached to the wrist over the radial artery. Afterward, the subjects were told to keep their palm facing up and slightly hyperextended to help expose the radial artery on the surface of the skin. Subjects were sitting up with the pressure sensor close to heart level during these measurements. No allergic reactions or pain was reported by the subjects tested.

For arterial pulse measurements, the pressure sensor was mounted onto an acrylic backing with a Velcro strap. A screw was attached to the acrylic backing such that the acrylic backing can apply incremental pressure to applanate the radial artery. The incremental pressure increased the baseline capacitance of the capacitive pressure sensor. The schematic illustration for the pressure sensor device can be seen in Figure 1. Medical tape, Tegaderm (3M Health Care) was also attached to the wrist to improve contact between the pressure sensor and the human skin. Lastly, a PDMS spacer (250 µm) was also used between the pressure sensor and the epidermis to further compress the tissue and amplify the radial arterial pulse. As blood pressure increases in the radial artery, the radial artery expands deforming the surrounding tissue, subsequently deforming the pressure sensor as seen in Figure 1e. This pressure can be related to arterial blood pressure as long as the contact between the pressure sensor and the body is consistently maintained.

To evaluate the capacitive pressure sensor's ability to measure beat-to-beat blood pressure, the pressure sensor was compared against an FDA approved finger volume clamp device, Clearsight (Edwards Lifesciences, Irvine, CA). The Clearsight was attached to the right index finger of the subject. A photographic image showing where the devices were attached can be seen in Figure S7 in the Supporting Information. Measurements were taken simultaneously where the pressure sensor measured the pressure exerted by the radial artery and the Clearsight measured brachial arterial pressure. An example of the radial arterial pulse waveforms measured from the pressure sensor and the Clearsight is presented in Figure 4a. As seen in Figure 4b, the quick response time and pressure sensitivity allowed for detection of the unique features in the radial arterial pulse waveform including the late systolic peak, which is not easily discernible in the Clearsight signal.

The parameters that were investigated included systolic (SBP), diastolic (DBP), and mean arterial pressures (MAP). These parameters are the most common when evaluating a

person's cardiovascular health. The SBP is the blood pressure against the arterial walls when the heart has contracted, the DBP is the blood pressure against the arterial walls when the heart has relaxed, and the MAP is the average pressure throughout one cardiac cycle and can be calculated using Equation (4)[38]

$$MAP = DBP + \frac{1}{3}(PP) \tag{4}$$

where PP is the pulse pressure, which is equal to SBP minus DBP.

As stated earlier, the arterial pulse can be palpated at many different regions on the human body. Research has shown that these arterial pulses have different waveforms as it propagates to different areas in the cardiovascular tree.[38–40] As blood is pumped from the heart, to the peripheral arteries, the arterial pulse waveform is amplified due to narrowing of blood vessels. By measuring these arterial pulse pressures, it is possible to then use that information as a proxy to estimate arterial pulse pressure at different locations in the cardiovascular tree.

The Clearsight measures the finger arterial pressure to estimate the brachial blood pressure. Extensive studies have evaluated the performance of the Clearsight device in a wide population range and have shown satisfactory results in accurately and precisely measuring brachial arterial pressure when compared against the radial arterial catheter—the gold standard for measuring beat-to-beat blood pressure. However, it is important to note that these studies have also shown variable results in patients, particularly when measuring systolic blood pressures.[8,41]

2.3.2. Beat-to-Beat Blood Pressure Data Analysis

When the Clearsight begins taking measurements, the Clearsight measures 10 cardiac cycles before a calibration step begins. After self-evaluation in accuracy, the Clearsight then measures 20 cardiac cycles and repeats the calibration step. The Clearsight will continue to measure additional cardiac cycles until it has reached 70 cardiac cycles at which the Clearsight is considered to be the most accurate and precise in measuring blood pressure. These epoch regions were where the capacitive pressure sensors were compared against the Clearsight.

In addition, subjects were asked to alternate between breathing deeply and normally after each subsequent 70 beat section, respectively. By breathing deeply, it is possible to increase blood pressure due to slight heart compression from lung expansion.[42] Subjects were asked to breathe deeply to assess the soft capacitive pressure sensor's ability to track larger changes in blood pressure.

Figure 4a,b illustrates the data collected for one subject. The remaining subject data can be seen in Tables S1–S3 in the Supporting Information. In Figure 4a, qualitative analysis shows that the two devices measured similar trends in blood pressure. This is apparent during the deep breathing sections where low frequency blood pressure changes are reflected in both the pressure sensor and Clearsight.

The SBP, DBP, and MAP were subsequently plotted against each other and analyzed using linear regression, as seen in Figure 4b. The goodness of fit between the pressure sensor and Clearsight device showed strong correlation with $R^2 = 0.765$ for SBP, $R^2 = 0.902$ for DBP, and $R^2 = 0.839$ for MAP. As stated earlier, previous studies show that the Clearsight device has difficulties in measuring accurate and precise SBP values, which could explain the lower R^2 between the pressure sensor and the Clearsight.[8,43–45]

To further assess the accuracy and precision of the pressure sensor's ability to monitor beat-to-beat blood pressure, the pressure sensor was calibrated to the Clearsight to generate a model for the pressure sensor and cross validated. To create the model, three consecutive cardiac cycles were first averaged together. After averaging, 75% of the data was randomly selected to generate a linear regression model for the pressure sensor. The remaining withheld dataset from the pressure sensor was converted to units of blood pressure–millimeters of mercury (mmHg). An example of this calibration from one subject is shown in **Figure 5**a–c.

Bland–Altman analysis was then used to assess the agreement in measurements of blood pressure between the pressure sensor and Clearsight.[46] Bland–Altman looks at the difference in blood pressures that were measured at the same time plotted against the average of the blood pressure measured at the same time. Larger differences would indicate larger disagreement between the two devices. As shown in Figure 5d, all seven subjects are compiled into one Bland–Altman plot including data sets from Subject 1 that was tested with two additional sensors. Mean bias and standard deviation calculated was −0.054 ± 2.09 mmHg. The ISO 81060–2 set by the AAMI has indicated that a NIBP is deemed interchangeable with an arterial catheter if mean biases are less than 5 mmHg with standard deviations of less than 8 mmHg.[8,47] The Bland–Altman analysis here shows that the mean bias and standard deviation are well below the requirements indicated by the ISO standards. Tables S4 and S5 in the Supporting Information also show the mean bias and standard deviations calculated with no averaging of cardiac cycles, which also show that the pressure sensor is well within the ISO standards. This suggests that the pressure sensor is highly accurate and precise in measuring blood pressure when calibrated to the Clearsight device. However, it is important to note that the ISO standards require that NIBP devices be directly compared against an arterial catheter and not against other NIBP devices. Future studies are therefore required to compare against the gold standard, arterial catheter.

The soft capacitive pressure sensors show strong evidence that radial tonometry is a feasible method for beat-to-beat NIBP monitoring. The capabilities to accurately monitor a wide range of pressures are enabled by the electromechanical properties of the pressure sensor. In addition, the quick response times of the capacitive pressure sensors allowed for detecting the radial arterial pulse waveform with high fidelity allowing for accurate and precise measurements of blood pressure.

3. Conclusion

Here, we have shown a facile method to develop a soft capacitive pressure sensor that has favorable electromechanical properties for measuring arterial pulsatile blood flow. By utilizing soft,
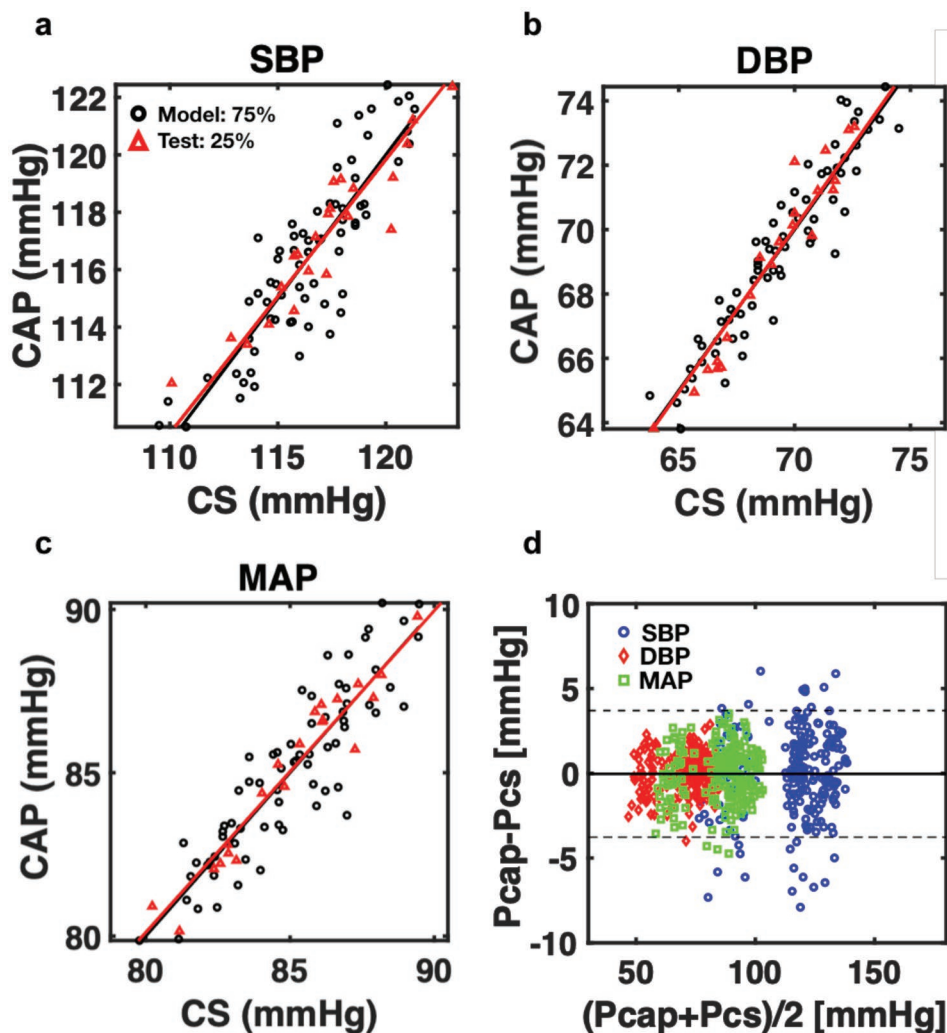
Figure 5. Example of pressure sensor calibration model from Subject 1 for a) SBP b) DBP, and c) MAP. d) Bland–Altman plot for all subjects combined. Data includes the different sensors used on Subject 1 for a total of nine independent tests. Dashed lines indicate two standard deviations and solid indicates mean bias.

highly wrinkled thin film electrodes, it was possible to fabricate soft pressure sensors with a large dynamic range that can couple effectively with the human body for the quantification of localized and subtle pressure. The sensors also demonstrated sufficient pressure sensitivities, quick response times, as well as mechanical robustness to cyclic loads.

We have demonstrated that these soft capacitive pressure sensors can be utilized for radial arterial tonometry applications. We report that consistent measurements of the arterial pulse pressure allowed for tracking and detecting nominal changes in SBP, DBP, and MAP pressures. Correlation between the FDA approved Clearsight device show promising results for potential ambulatory beat-to-beat NIBP monitoring. The quick response times and wide dynamic range of the soft capacitive sensors allow detection of rapid and large changes in blood pressure that are essential for monitoring acute cardiovascular events. The next step is to further evaluate the capacitive pressure sensors by comparing against the radial arterial catheter with a larger and broader population.

4. Experimental Section

Fabrication of Capacitive Based Pressure Sensor: The sensor was comprised of four layers: a wrinkled electrode, a dielectric layer, an air gap, and a wrinkled electrode with etched ridges. To fabricate the electrodes, both processes began with rinsing a prestressed PS substrate (Grafix Shrink Film KSF50-C, Grafix Arts, OH) with 70% ethanol. The sensor design was developed using AutoCAD (Autodesk, Inc., CA), and patterned onto a shadow mask made with an adhesive polymer film (Grafix Frisket Film, Grafix Arts, OH) with a laser cutter (Universal Laser, AZ). Design was drawn such that the final electrode dimensions after shrinking were 2 mm in width and 15 mm in length. The Frisket film was first placed on top of the PS substrate, and the sensor design was then patterned onto the masked PS substrate. For the electrode with etched ridges, a higher power setting (0.5% power, 3% speed, 1000 PPI) was used to etch along the side of the electrode into the PS substrate. After both substrates were masked and patterned, a magnetron sputter coater (Q150R, Quorum Technologies, UK) was used to deposit 15 nm of Au onto each PS substrate. Subsequently, the shadow mask was removed, and the sputtered substrate was placed into a convection oven at 140 °C to induce biaxial shrinking and wrinkling of the Au film. The shrunken samples were treated with 5×10^{-3} M of 3-mercaptopropyl

trimethoxysilane (95% MPTMS, Sigma Aldrich) in pure ethanol for 1 h. The samples were then rinsed with ethanol and dried with an air gun. Afterward, PDMS (Sylgard 184 Silicone Elastomer Base, Dow Corning, MI) was poured over the MPTMS-treated Au film and spin coated at 300 rpm for 30 s with a final substrate thickness of ≈0.5 mm. The samples were placed in a vacuum 30 min to remove bubbles and cured overnight in a convection oven at 60 °C. The cured samples were then placed in a 75 °C acetone bath for 15 min to dissolve the PS substrate and lift the PDMS and wrinkle Au film off the PS. Afterward, the residual PS was cleaned off of the wrinkled thin film by submerging the sensor in toluene for 2 min and rinsing with acetone. The samples were then air dried for overnight. Colloidal silver liquid (Pelco Colloidal Silver Liquid, Ted Pella, CA) was used to interconnect the Au electrode to a wire and after drying, a resin was used encapsulate the interconnect interface. After the resin dried, polyimide tape was placed on the resin to further secure the interconnect to the electrode. Ecoflex cannot be immediately plasma bonded to PDMS substrates without additional steps. Ecoflex can only be plasma bonded to other silicones when Ecoflex is cured on a PDMS substrate or chemically modified with other silicone elastomers.[48] Therefore, a silicone elastomer Ecoflex 0030 (Smooth-On, PA) was first spin coated onto a cured PDMS layer with a spread step of 1000 rpm for 10 s, and spin coat step of 3000 rpm for 30 s for a final thickness of 15 µm. The elastomer was then placed into a 60 °C convection oven for 2 h to cure. Next, the cured elastomer was plasma bonded to the flat electrode at ≈120 mTorr with ambient air for 40 s (PE-50, Plasma Etch, NV) and then placed in a 60 °C convection oven to promote chemical bonding. After removing the PDMS layer from the Ecoflex layer, the flat electrode with the dielectric layer was then plasma bonded to the etched electrode to form the final capacitive based sensor. The sensor was placed into a convection oven at 60 °C to promote chemical bonding.

Flat Au electrodes (which served as the controls) were fabricated by patterning 90 nm Au onto a PS substrate. The Au was treated with 5×10^{-3} M MPTMS (95% MPTMS) in pure ethanol for 1 h. PDMS was then spin coated at 300 rpm for 30 s on substrate and cured in the convection oven at 60 °C for 2 h. Acetone drops were placed on the PDMS to lift the Au from the PS substrate. After attaching electrical interconnects, Ecoflex 0030 was spin coated on one electrode at 3000 rpm for 30 s and then cured in 60 °C convection oven for 2 h. After curing, counter electrode was placed on top of the electrode with Ecoflex dielectric layer. Surface area overlap of the electrodes was 2×2 mm^2.

Characterization: A scanning electron microscope (SEM) (FEI Magellan 400 XHR) was used to characterize the wrinkle structures in the Au film. Pressure sensitivity was tested using a force gauge (Force Gauge Series 5, Mark-10, NY) connected to a test stand (ESM303, Mark-10, NY). The force gauge was placed slightly above the sensor, then moved with a down speed of 1.1 mm min^{-1} with a force probe diameter of 6 mm. Fiber glass probe was used to reduce fringe effects. The change in capacitance was collected as force was being applied and measured with an LCR meter (300 kHz) (E4980AL Precision LCR Meter, Keysight, CA). Data was collected using LabView and then processed using Matlab. An impedance analyzer (1 MHz, 500 mV) (4291B, Agilent, CA) was used to measure the signal response of the pressure sensor from cyclic and static loading applied by a custom-made linear actuator controlled by an Arduino. Distance information from the custom-made linear actuator was recorded with a linear potentiometer (Spectra Symbol, UT) using a National Instrument data acquisition system (USB-6003, TX).

Beat-to-Beat Blood Pressure Methods: The sensor was assembled onto a custom-made Velcro band with a screw to incrementally apply pressure. Prior to attaching the sensor to the body, a Tegaderm (3M Health Care, MN) strip was placed on the left wrist to promote compatibility between sensor and skin. The sensor was then attached and strapped down with custom made Velcro band. The Clearsight finger cuff was attached to the right index finger of the subject. Measurements between the pressure sensor and the Clearsight device was measured simultaneously and subsequently analyzed in Matlab. All subjects in this study gave their informed consent.

Statistical Analysis: The sensor capacitance readings were acquired with a sampling frequency of ≈56 Hz from the LCR meter (data points were timestamped with millisecond precision). All datasets were post-processed in Matlab and linearly interpolated to 200 Hz to match that of Clearsight (200 Hz). The interpolated data were then smoothed with a moving average filter of five data points.

As mentioned earlier, the Clearsight segments the beat-to-beat blood pressure measurements by the number of cardiac cycles detected. Sections consisting of 70 beats were regarded as the most accurate and precise in measuring blood pressure. However, each of these sections only contained 69 full cardiac cycles, which were used for the analysis. Different breathing maneuvers were performed in four consecutive sections. Linear regression between the pressure sensor and Clearsight for SBP, DBP, and MAP ($n = 69$) for each subject and individual sections were obtained. The four sections for each subject were then combined and analyzed with linear regression ($n = 276$).

Bland–Altman analysis was used to investigate agreement between the Clearsight and the pressure sensor. The data from each subject were randomly split into two independent sets, where 75% of the data were used for creating the model and 25% were used to test the model. Linear regression models were built to predict SBP, DBP, and MAP values, respectively ($n = 207$). The remaining data for each subject ($n = 69$) were then calibrated with the linear regression models. The mean bias and standard deviation were then calculated for all nine subject tests combined for each SBP, DBP, and MAP parameter ($n = 621$). Three consecutive cardiac cycles were averaged and analyzed similarly ($n = 207$). Mean bias and standard deviation were calculated for all SBP, DBP, and MAP parameters combined for no cardiac cycle averaging ($n = 1863$) and also for three consecutive cardiac cycle averaging ($n = 621$).

Supporting Information

Supporting Information is available from the Wiley Online Library or from the author.

Conflict of Interest

The authors declare no conflict of interest.

[1] J. F. Moran, *Pulse*, Butterworths, Boston **1990**.
[2] P. Verdecchia, C. Porcellati, G. Schillaci, C. Borgioni, A. Ciucci, M. Battistelli, M. Guerrieri, C. Gatteschi, I. Zampi, A. Santucci, C. Santucci, G. Reboldi, *Hypertension* **1994**, *24*, 793.
[3] G. Mancia, G. Parati, M. Hennig, B. Flatau, S. Omboni, F. Glavina, B. Costa, R. Scherz, G. Bond, A. Zanchetti, *J. Hypertens.* **2001**, *19*, 1981.

[4] R. A. V. Irtanen, A. N. J. Ula, J. O. K. S. Alminen, L. I. Aria, V. O. Ulkki, *Psychosom. Med.* **2003**, *65*, 751.

[5] A. J. S. Webb, S. Mazzucco, L. Li, P. M. Rothwell, *Stroke* **2018**, *49*, 62.

[6] E. Pringle, C. Phillips, L. Thijs, C. Davidson, J. A. Staessen, P. W. De Leeuw, M. Jaaskivi, C. Nachev, G. Parati, E. T. O. Brien, J. Tuomilehto, J. Webster, *J. Hypertens.* **2003**, *21*, 2251.

[7] P. Bovet, P. Hungerbuhler, J. Quilindo, M. Grettve, B. Waeber, B. Burnand, *Hypertension* **1994**, *24*, 786.

[8] K. Lakhal, S. Ehrmann, T. Boulain, *Chest* **2018**, *153*, 1023.

[9] A. S. Meidert, B. Saugel, *Front. Med.* **2018**, *4*, 231.

[10] E. Chung, G. Chen, B. Alexander, M. Cannesson, *Front. Med.* **2013**, *7*, 91.

[11] J. Penáz, A. Voigt, W. Teichmann, *Z. Gesamte Inn. Med. Ihre Grenzgeb.* **1976**, *31*, 1030.

[12] H.-M. Cheng, D. Lang, C. Tufanaru, A. Pearson, *Int. J. Cardiol.* **2013**, *167*, 1867.

[13] M. R. Nelson, J. Stepanek, M. Cevette, M. Covalciuc, R. T. Hurst, A. J. Tajik, *Mayo Clin. Proc.* **2010**, *85*, 460.

[14] N. Luo, W. Dai, C. Li, Z. Zhou, L. Lu, C. C. Y. Y. Poon, S. C. Chen, Y. Zhang, N. Zhao, *Adv. Funct. Mater.* **2016**, *26*, 1178.

[15] C. Dagdeviren, Y. Su, P. Joe, R. Yona, Y. Liu, Y.-S. Kim, Y. Y. Huang, A. R. Damadoran, J. Xia, L. W. Martin, J. A. Rogers, *Nat. Commun.* **2014**, *5*, 4496.

[16] J. Yang, J. Chen, Y. Su, Q. Jing, Z. Li, F. Yi, X. Wen, Z. Wang, Z. Lin Wang, J. Yang, J. Chen, Y. Su, Q. Jing, Z. Li, F. Yi, X. Wen, Z. Wang, Z. L. Wang, *Adv. Mater.* **2015**, *27*, 1316.

[17] K. Meng, J. Chen, X. Li, Y. Wu, W. Fan, Z. Zhou, Q. He, X. Wang, X. Fan, Y. Zhang, J. Yang, Z. L. Wang, *Adv. Funct. Mater.* **2018**, *29*, 1806388.

[18] C. Pang, J. H. Koo, A. Nguyen, J. M. Caves, M.-G. Kim, A. Chortos, K. Kim, P. J. Wang, J. B.-H. Tok, Z. Bao, *Adv. Mater.* **2015**, *27*, 634.

[19] S. Hwan Cho, S. Won Lee, S. Yu, H. Kim, S. Chang, D. Kang, I. Hwang, H. Sol Kang, B. Jeong, E. Hyuk Kim, S. Man Cho, K. Lib Kim, H. Lee, W. Shim, C. Park, *ACS Appl. Mater. Interfaces* **2017**, *9*, 10128.

[20] Y. Joo, J. Yoon, J. Ha, T. Kim, S. Lee, B. Lee, C. Pang, Y. Hong, *Adv. Electron. Mater.* **2017**, *3*, 1600455.

[21] Z. He, W. Chen, B. Liang, C. Liu, L. Yang, D. Lu, Z. Mo, H. Zhu, Z. Tang, X. Gui, *ACS Appl. Mater. Interfaces* **2018**, *10*, 12816.

[22] B. Zhuo, S. Chen, M. Zhao, X. Guo, *IEEE J. Electron Devices Soc.* **2017**, *5*, 219.

[23] R. Li, Y. Si, Z. Zhu, Y. Guo, Y. Zhang, N. Pan, G. Sun, T. Pan, *Adv. Mater.* **2017**, *29*, 1700253.

[24] D. J. Lipomi, M. Vosgueritchian, B. C.-K. Tee, S. L. Hellstrom, J. A. Lee, C. H. Fox, Z. Bao, *Nat. Nanotechnol.* **2011**, *6*, 788.

[25] S. C. B. Mannsfeld, B. C.-K. Tee, R. M. Stoltenberg, C. V. H.-H. Chen, S. Barman, B. V. O. Muir, A. N. Sokolov, C. Reese, Z. Bao, *Nat. Mater.* **2010**, *9*, 859.

[26] G. L. Pressman, P. M. Newgard, *IRE Trans. Bio-Med. Electron.* **1963**, *10*, 73.

[27] G. Drzewiecki, G. Krishna, H. Katta, *Comput. Biol. Med.* **2019**, *104*, 329.

[28] J. Kim, S.-J. J. Park, T. Nguyen, M. Chu, J. D. Pegan, M. Khine, *Appl. Phys. Lett.* **2016**, *108*, 061901.

[29] J. D. Pegan, J. Zhang, M. Chu, T. Nguyen, S.-J. Park, A. Paul, J. Kim, M. Bachman, M. Khine, *Nanoscale* **2016**, *8*, 17295.

[30] S. J. Park, J. Kim, M. Chu, M. Khine, *Adv. Mater. Technol.* **2016**, *1*, 1600053.

[31] T. H. N. Dinh, E. Martincic, E. Dufour-Gergam, P. Y. Joubert, *J. Sens.* **2017**, *2017*, 1.

[32] P. Maiolino, F. Galantini, F. Mastrogiovanni, G. Gallone, G. Cannata, F. Carpi, *Sens. Actuators, A.* **2015**, *226*, 37.

[33] M. Liu, J. Sun, Y. Sun, C. Bock, Q. Chen, *J. Micromech. Microeng.* **2009**, *19*, 035028.

[34] I. D. Johnston, D. K. McCluskey, C. K. L. Tan, M. C. Tracey, *J. Micromech. Microeng.* **2014**, *24*, 035017.

[35] M. Kubo, X. Li, C. Kim, M. Hashimoto, B. J. Wiley, D. Ham, G. M. Whitesides, *Adv. Mater.* **2010**, *22*, 2749.

[36] J. Wang, J. Jiu, M. Nogi, T. Sugahara, S. Nagao, H. Koga, P. He, K. Suganuma, *Nanoscale* **2015**, *7*, 2926.

[37] J. Diani, B. Fayolle, P. Gilormini, *Eur. Polym. J.* **2009**, *45*, 601.

[38] D. Unglaub Silverthorn, *Human Physiology: An Integrated Approach*, Pearson, London **2013**, p. 568.

[39] G. M. London, A. P. Guerin, *Am. Heart J.* **1999**, *138*, S220.

[40] K. Takazawa, H. Kobayashi, N. Shindo, N. Tanaka, A. Yamashina, *Hypertens. Res.* **2007**, *30*, 219.

[41] R. B. P. de Wilde, F. de Wit, B. F. Geerts, A. L. van Vliet, L. P. H. J. Aarts, J. Vuyk, J. R. C. Jansen, *Anaesthesia* **2016**, *71*, 788.

[42] V. Novak, P. Novak, J. De Champlain, A. R. Le Blanc, R. Martin, R. Nadeau, *J. Appl. Physiol.* **1993**, *74*, 617.

[43] P. Schramm, I. Tzanova, T. Gööck, F. Hagen, I. Schmidtmann, K. Engelhard, G. Pestel, *J. Neurosurg. Anesthesiol.* **2017**, *29*, 251.

[44] F. Balzer, M. Habicher, M. Sander, J. Sterr, S. Scholz, A. Feldheiser, M. Müller, C. Perka, S. Treskatsch, *J. Int. Med. Res.* **2016**, *44*, 832.

[45] J. F. Heusdens, S. Lof, C. W. A. Pennekamp, J. C. Specken-Welleweerd, G. J. de Borst, W. A. van Klei, L. van Wolfswinkel, R. V. Immink, *Br. J. Anaesth.* **2016**, *117*, 316.

[46] J. Martin Bland, D. Altman, *Lancet* **1986**, *327*, 307.

[47] K. Lakhal, M. Martin, S. Ehrmann, T. Boulain, *Eur. J. Anaesthesiol.* **2015**, *32*, 367.

[48] D. Sritharan, E. Smela, *Polymers.* **2016**, *8*, 400.

1900109 (9 of 9)